



Visible light-active pure and lanthanum-doped copper oxide nanostructures for photocatalytic degradation of methylene blue dye and hydrogen production

Muhammad Rafique¹  | N. R. Khalid² | Muneeb Irshad³ | Falak Shafiq⁴ |
 Muhammad Usman⁵ | Yasser Fouad⁶ | Muhammad Imran^{7,8} |
 Mohammad A. Assiri^{7,8} | Waqar Muhammad Ashraf⁹ 

¹Department of Physics, University of Sahiwal, Sahiwal, Pakistan

²Department of Physics, University of Okara, Okara, Pakistan

³Department of Physics, University of Engineering and Technology, Lahore, Pakistan

⁴Department of Physics, Faculty of Science, University of Gujrat, Gujrat, Pakistan

⁵Department of Mechanical Engineering, University of Engineering and Technology, Lahore, Pakistan

⁶Department of Applied Mechanical Engineering, College of Applied Engineering, Muzahimiyah Branch, King Saud University, Riyadh, Saudi Arabia

⁷Research Centre for Advanced Materials Science (RCAMS), King Khalid University, Abha, Saudi Arabia

⁸Department of Chemistry, Faculty of Science, King Khalid University, Abha, Saudi Arabia

⁹Department of Chemical Engineering, Sargent Centre for Process Systems Engineering, University College London, London, UK

Correspondence

Muhammad Rafique, Department of Physics, University of Sahiwal, Sahiwal 57000, Pakistan.

Email: mrafique.uet@gmail.com and mrafique@uosahiwal.edu.pk

Waqar Muhammad Ashraf, Department of Chemical Engineering, Sargent Centre for Process Systems Engineering, University College London, Torrington Pl, London WC1E 7JE, UK.

Email: waqar.ashraf.21@ucl.ac.uk

Funding information

National Plan for Science, Technology and Innovation, Grant/Award Number: RSPD2023R698

Abstract

Clean water and renewable energy sources are becoming increasingly important in the current era, as well as a future challenge, and one of the potential solutions is photocatalysis. In the current study, a simple one-step hydrothermal technique is employed to fabricate the pure and La-doped CuO (0%, 1%, 3%, 5%, and 7%) photocatalysts. The influence of varying La concentration on structure, morphology, and optical properties is determined by scanning electron microscope (SEM), X-ray diffraction (XRD), ultraviolet (UV)-visible spectroscopy, and photoluminescence. SEM showed that synthesized nanostructures are irregularly spherical and transform into needle-like nanostructures on increasing La concentration. XRD revealed the monoclinic phase with a crystallite size of 15–23 nm. The UV-visible spectrum exhibited a decrease in the band gap of La-doped CuO needle-like nanostructures from UV to visible light. The composition and purity of synthesized nanostructures are evaluated via the energy-dispersive X-ray spectrum which revealed that needle-like nanostructures are pure without any impurity traces. The synthesized nanostructures were used as a photocatalyst

This is an open access article under the terms of the Creative Commons Attribution License, which permits use, distribution and reproduction in any medium, provided the original work is properly cited.

© 2023 The Authors. *Energy Science & Engineering* published by Society of Chemical Industry and John Wiley & Sons Ltd.

against methylene blue dye to examine their photocatalytic activity. The synthesized CuO-3La photocatalyst exhibited excellent photocatalytic performance of dye degradation and hydrogen production $95.3 \mu\text{mol h}^{-1} \text{g}^{-1}$ with more than 97% cyclic stability. Therefore, the synthesized La-doped CuO nanostructures are potential candidates for photocatalytic water splitting and hydrogen evolution.

KEYWORDS

dye degradation, hydrogen energy, metal oxide, photocatalysis, wastewater treatment

1 | INTRODUCTION

The fast population growth, depletion of clean water resources, and prolonged floods and droughts caused by climate change have made clean water a precious resource in many regions of the world.¹ Alongside, environmental effluents are posing critical health issues to living beings at a massive scale overall the globe. These effluents are being manufactured via different resources, that is, paper making and printing industries, pharmaceuticals, textiles, and so forth. Clean water, one of the major living sources for the individuals on earth, is adversely affected due to these effluents over a large scale. It is necessary to have clean water, free from any kind of contaminants, for worldwide wellbeing.^{2,3} It has become mandatory to develop appropriate technologies to manage and treat these effluents efficiently from wastewater.^{4,5} Also, conventional wastewater treatment technologies have lost their impact due to the fact that these methods convert pollutants from one form to another, in turn generate secondary pollutants, and require another treatment.^{6,7} Currently, advanced oxidation process has appeared as a potential catalytic process that completely degrades a wide range of pollutants. This method has a breakthrough due to the fact that nontoxic and cheap nanomaterials have been utilized for the pollutant's reduction.^{8–10} On the other hand, to overcome future energy crisis, hydrogen (H_2) is considered as a sustainable and clean energy resource and photocatalytic nanomaterials exhibiting promising results for H_2 energy production.¹¹

In the past few decades, with an increased focus on the characteristics, copper (II) oxide (CuO) has been investigated extensively.¹² CuO, a semiconducting material, possesses a narrow band gap in bulk and wide band gap as nanomaterials and is widely used in numerous applications, such as in photocatalytic^{13,14} and catalytic processes,^{15,16} capacitors,^{17,18} sensors,¹⁹ solar cells,²⁰ batteries,²¹ and storage media.²² Further, CuO appertains to the imperious group of environmental catalyts

utilized for discarding a number of synthetic and organic pollutants.²³

The photocatalytic characteristics eminently rely on the underlying characteristics of photocatalyst material and are intensely influenced by the particle shape, size, surface area, exposed crystal face, band gap, and so forth.²⁴ The capability to govern synthesis factors such as pressure, temperature, reaction time as well as concentration of reactant is essential for assuring the desired characteristics for the final product, therefore, the synthetic method also plays a crucial role.²⁵ The incorporation of certain elements (cations) or materials into compound crystal structure also brings significant changes in optical, morphological, and structural characteristics along with grain size and particle reactivity.²⁶ A number of chemical methods such as electrochemical,²⁷ thermal, solution-based chemical precipitation,²⁸ and hydrothermal²⁹ methods have been established for the fabrication of CuO. The hydrothermal method utilized in the current work is considered as an easy, cost-effective, and time-saving method. This synthesis method also proposes large opportunities for doping of materials and thus altering essential characteristics. A material with higher catalytic properties can be certainly synthesized by combining the aforementioned techniques. In our photocatalytic evaluation, methylene blue (MB) dye is used whose high concentrations are toxic to living beings.

There is only limited literature on lanthanum (La)-doped CuO. Lanthanum, an abundant rare earth element with silvery white physical appearance,³⁰ as an incorporating material. La is being used as a catalyst as well as its ability to improve the catalytic performance of other materials when used as an additive.³¹ There are some other metal oxides that have been reported with La doping in recent studies. Jian et al. claimed the synthesis of La-doped ZnO nanofibers for exceptional photocatalytic activity under visible light irradiation.³² Varughese et al. fabricated La-doped CuO via chemical precipitation route to explore the optical properties of CuO:La

nanostructures.³³ Devi et al. synthesized the LaCuO via solution combustion technique to investigate the photoluminescence (PL) properties as well as to study lattice defects.³⁴ Devi et al. explored the optical and structural properties of La-doped CuO for different concentration and annealing temperatures, fabricated via solution combustion technique.³⁵ Yan et al. fabricated La-doped CuO via electrodeposition route to explore the photocatalytic reduction of MB dye which was 11.5% greater than pure CuO.³⁶ Rodney et al. synthesized La-doped CuO prepared via solution combustion approach for observing the efficient photocatalytic evaluation of MB dye which was 98%.³⁷ However, fluorides removal activity have also been evaluated in some recent studies^{31,38,39}

In the present study, La-doped CuO nanostructures were fabricated first time via a simple, easy-to-handle, and inexpensive hydrothermal route. The fabricated final product was characterized by different techniques, and doping influence on optical, structural, and morphological properties was studied. An easy route is followed to evaluate the photocatalytic characteristics of prepared La-doped CuO on MB dye and efficient H₂ energy production.

2 | EXPERIMENTAL

2.1 | Material and method

Analytical grade Cu(NO₃)₂·3H₂O (≥99.5), La(NO₃)₃·6H₂O (≥99.5), and NaOH (≥98) were bought from Sigma Aldrich and were used without further process. The pure CuO- and La-doped CuO nanostructures were fabricated via a facile hydrothermal technique.

2.2 | Synthesis

An aqueous solution of the precursor (6.6 g, Cu(NO₃)₂·3H₂O) was prepared in 1000 mL deionized water, and the corresponding amount of La(NO₃)₃·6H₂O with molar ratios of 0%, 1%, 3%, 5%, and 7% was added while vigorously stirring. The solution was stirred continuously for 20 min without heating, and NaOH was inserted dropwise to maintain the desired pH. Then, this solution was placed into a Teflon-lined (stainless steel) autoclave and solution was allowed to react for 24 h at 160°C. After the reaction, the solution was allowed to cool down to room temperature. Distilled water was employed to wash the precipitates several times that are further filtered and dried at 100°C. In addition, the powder was calcined at 400°C for 3 h. The obtained samples were named as pure CuO, CuO-1La, CuO-3La, CuO-5La, and CuO-7La. A flow diagram of the synthesis mechanism of CuO-La as-synthesized nanostructures is depicted in Figure 1.

2.3 | Characterizations

The X-ray diffraction (XRD) spectra were acquired with a powder X-ray diffractometer (KAPPA APEX II, Cu-α, λ = 1.54 Å) for structural analysis. The XRD data were determined at a fast scan with a step size of 0.02. The morphological and elemental properties were analyzed via a scanning electron microscope (SEM) coupled energy-dispersive X-ray (EDX) spectroscopy (TESCAN MIRA3). Fourier transform infrared (FTIR) spectroscopy was utilized to track different functional groups and bonding. The optical properties, surface-plasmon-resonance and band gap, were investigated using an ultraviolet (UV)-visible spectrophotometer (UV-1800,

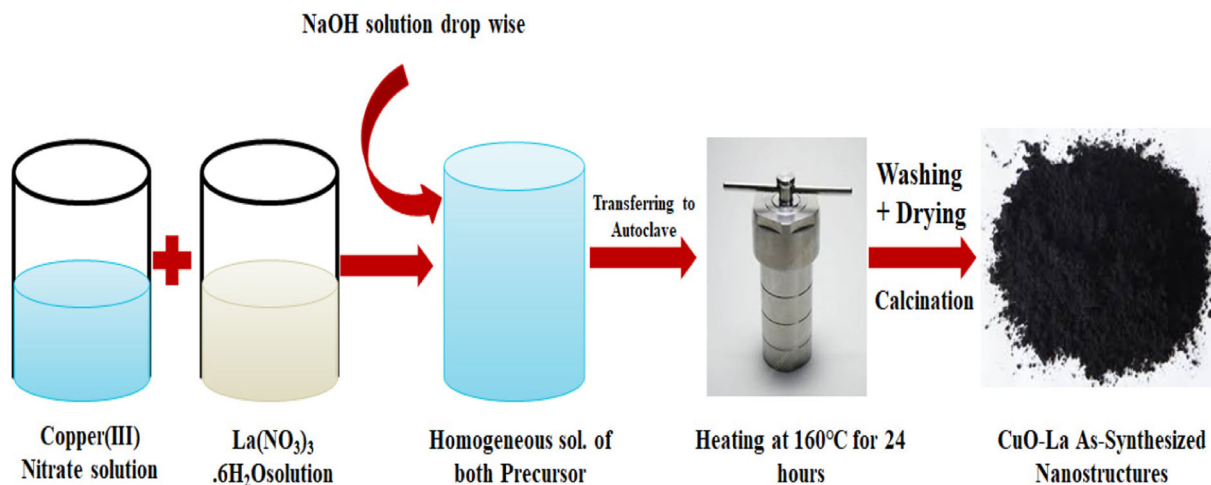


FIGURE 1 Flow diagram of synthesis mechanism of CuO-La nanostructures.

Shimadzu). PL spectroscopy (JASCO FP-8200) was used to examine the recombination rate of the synthesized nanostructures.

2.4 | Photocatalytic evaluation

Photocatalytic performance of the prepared pure CuO and CuO-La photocatalysts was performed against MB dye. For photocatalytic activity, 2.5 mg MB dye was suspended in 250 mL distilled water (for each set of experiments) and stirred well over a magnetic stirrer without heating. This dye solution was kept in the dark for several hours to get equilibrium. Photocatalytic reactor was employed to perform the photocatalytic activity under UV and visible light for various catalytic parameters, that is, catalyst loading, time, and pH.

The percentage dye degradation by the photocatalyst was calculated by Equation (1)^{40,41}:

$$\begin{aligned} \text{Percentage Dye Degradation} \\ = ((C_0 - C)/C_0) \times 100, \end{aligned} \quad (1)$$

whereas C_0 is the initial dye concentration at time $t = 0$ and C is the final dye concentration after a time interval t .

3 | RESULTS AND DISCUSSION

3.1 | Structural analysis

The XRD graph represents diffraction peaks at angles $2\theta = 32.3, 35.42, 38.84, 48.58, 58.24, 61.52, 68.1,$ and 75.04 corresponding to Bragg reflection plans (110), (111), (202), (202), (113), (311), and (220), respectively, of CuO. The monoclinic crystal system is well referenced to JCPDS card number 89-2531 having lattice parameters a (Å) = 4.6691, b (Å) = 3.4805, and c (Å) = 5.1183.^{42,43} The intensity and broadening of the diffraction peaks are attributed to the materials crystallinity. There were no impurity peaks in the CuO, CuO-1La, CuO-3La, and CuO-5La, however, in CuO-7La sample, there are some small peaks that are may be due to some new phase.

The normalized XRD graphs are shown in Figure 2 which can provide the comparison for the intensity and broadening of the diffraction peaks. It is clear from the graph that the peaks intensity decreases with the increase in doping. As the ionic radius of La is much higher than that of Cu, therefore incorporation of La ions into Cu cause a lattice expansion.⁴⁴ The diffraction plane 110 is

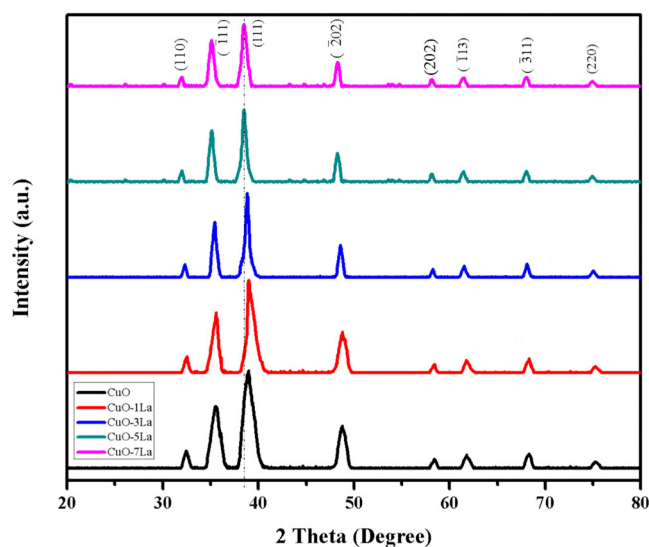


FIGURE 2 X-ray diffraction patterns of CuO, CuO-1La, CuO-3La, CuO-5La, and CuO-7La samples.

identified which is in accordance with the literature of nanomaterials.^{44,45}

The details obtained with XRD results were employed to calculate crystallites size from Debye–Scherrer formula given in Equation (2)⁴⁶:

$$D = \frac{k\lambda}{\beta \cos \theta}, \quad (2)$$

where D represents the crystallites size, k is the Debye–Scherrer constant, λ is the wavelength of X-rays incident on a sample having value 1.5406 Å (Angstrom), β is full-width at half-maximum, and θ is the diffraction angle. The average crystallite size having a range of 15 – 25 nm was obtained. XRD parameters, that is, peak positions, FWHM, and crystalline size for each peak of the as-synthesized are given in Table 1, for CuO, CuO-1La, CuO-3La, CuO-5La, and CuO-7La, respectively.

3.2 | Morphological analysis

The SEM analysis was used to examine morphology, that is, shape and size of synthesized nanostructures. The SEM micrographs of synthesized La-doped CuO nanostructures are displayed in Figure 3, where Figure 3A depicts an SEM micrograph of a CuO-1La sample with irregular and diffused rod-like morphology. Figure 3B represents an SEM image of a CuO-3La sample with needle-like morphology with a high surface area. Figure 3C depicts the SEM image of the CuO-5La sample with irregular, aggregated, and diffused nanostructures. It is clear that the doping of the La varied the

TABLE 1 XRD parameters of CuO, CuO-1La, CuO-3La, CuO-5La, and CuO-7La samples.

Peak position 2θ					FWHM					Crystallites size				
CuO-	CuO-1La	CuO-3La	CuO-5La	CuO-7La	CuO-	CuO-1La	CuO-3La	CuO-5La	CuO-7La	CuO-	CuO-1La	CuO-3La	CuO-5La	CuO-7La
32.45	32.5	32.3	31.98	31.97	0.66	0.55	0.32	0.34	0.33		15.81	26.99	25.39	
35.47	35.6	35.42	35.10	35.10	0.99	0.74	0.49	0.5	0.5	13.09	11.77	17.77	17.40	17.40
38.96	38.98	38.84	38.5	38.45	1.03	0.82	0.43	0.44	0.44	8.80	10.73	20.46	19.97	19.97
48.75	48.78	48.58	48.26	48.24	0.98	0.45	0.52	0.52	0.54	8.54	20.24	17.51	17.48	17.50
58.4	58.42	58.24	58.16	58.13	0.57	0.48	0.32	0.32	0.33	9.29	19.80	29.68	29.67	29.67
61.8	61.74	61.52	61.46	61.44	0.83	0.5	0.46	0.46	0.47	16.67	19.33	20.99	20.98	20.96
68.28	68.3	68.1	68.02	68.0	0.64	0.68	0.4	0.4	0.41	11.65	14.74	25.04	25.02	25.02
75.2	75.24	75.04	74.96	74.94	0.79	0.74	0.36	0.42	0.42	15.66	14.15	29.06	24.89	24.8

Abbreviations: FWHM, full-width at half-maximum; XRD, X-ray diffraction.

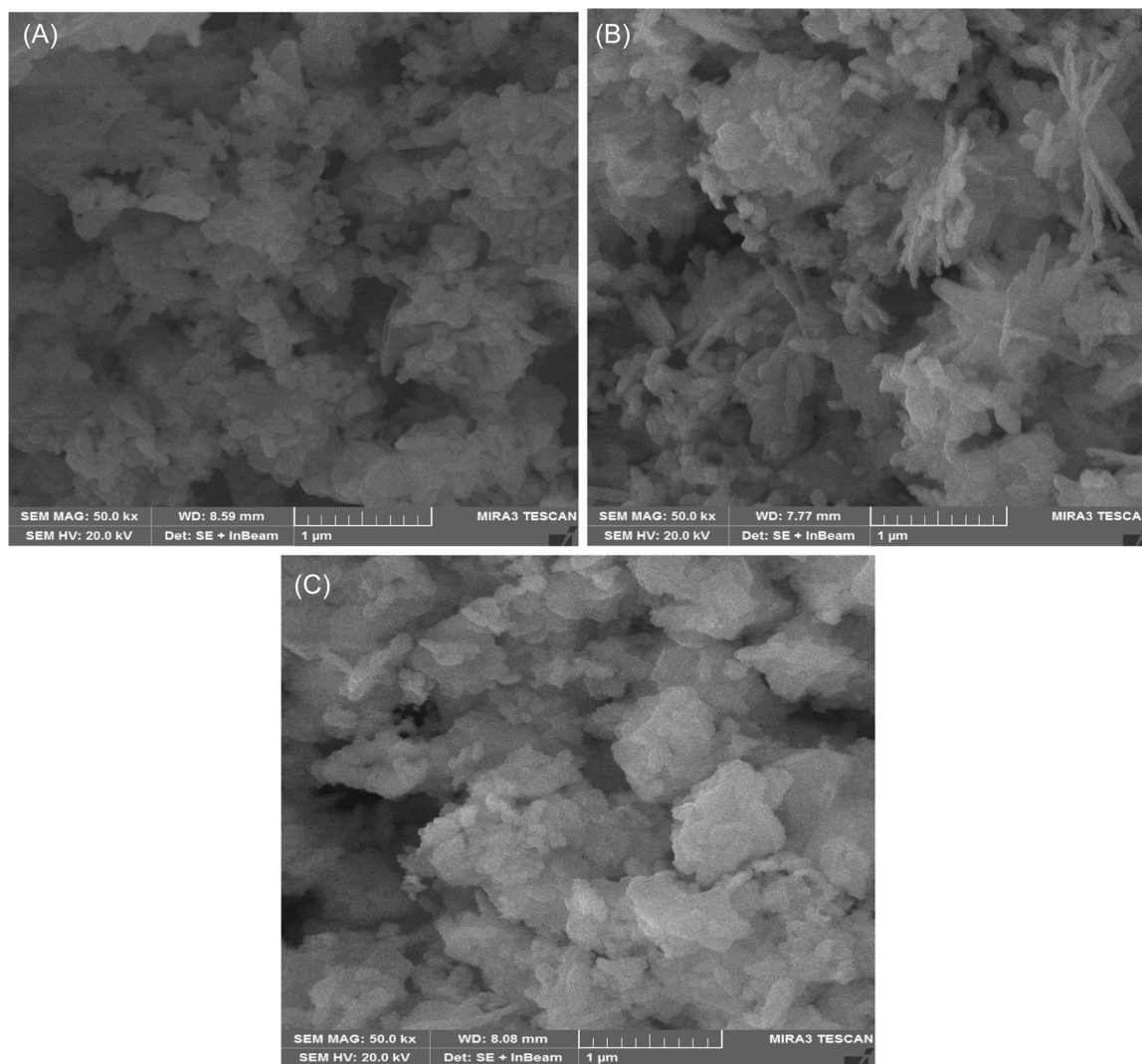


FIGURE 3 SEM images of La-doped CuO nanostructures. (A) CuO-1La sample, (B) CuO-3La sample, and (C) CuO-5La sample. SEM, scanning electron microscope.

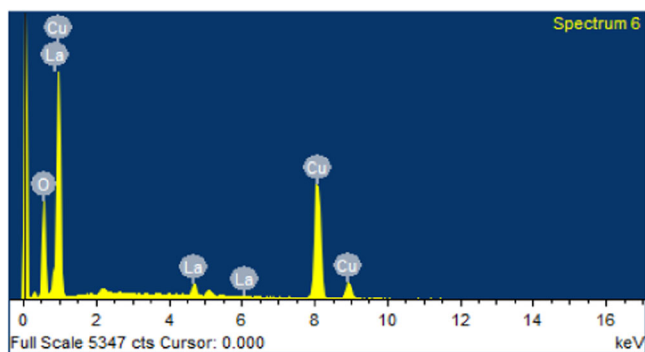


FIGURE 4 Energy-dispersive X-ray spectra of CuO-3La sample.

morphology, agglomeration, and size of the nanostructures. The structures and dimensions of the host materials are affected by the dopant concentrations and reaction parameters. The incorporation of La ions expands the CuO structure because of the difference, in both host as well as dopant, charges and sizes.⁴⁷

EDX spectrum of synthesized La-doped CuO nanostructures is given in Figure 4 which reveals the composition and purity of synthesized nanostructures. The spectrum also represents the Cu, La, and O as 73.96, 5.96, and 20.08 wt% and 47.29, 1.74, and 50.97 at%, respectively. The samples have no impurity traces and therefore can be tuned by the concentration of the dopants.

3.3 | FTIR analysis

FTIR spectra of pure CuO, and CuO-1La, CuO-3La, CuO-5La, and CuO-7La nanostructures are shown in Figure 5. Bands of vibrations below 1150 cm^{-1} are because of the interatomic vibrations that arise from the metal oxides. The absorption frequencies in the region between 585, 591, 599, 600, 608, and 668 cm^{-1} attributes to the bending and stretching of CuO molecules.^{38,48} O–H stretching vibration is due to the solvent (water) which is adsorbed on the surface of nanostructure from the air.^{14,49,50} It also has been observed that the incorporation of La ions in CuO brings a shift in the frequency bands of the undoped CuO.

3.4 | UV–visible analysis

Optical properties of fabricated pure CuO- and La-doped CuO nanostructures were explored via UV–visible spectroscopy technique by analyzing the colloidal solutions. The absorbance spectra of pure CuO- and La-doped

CuO nanostructures are depicted in Figure 6A. It is found that an increase in La doping concentration implies a red shift in peaks which also represents the decrease in the band gap of synthesized nanostructures. This reduction in band gap can be attributed to the formation of shallow states near the conduction band which reduces the band gap less as compared with pure matrix.³⁶ However, by increasing doping to a large extent can have a reverse effect on the band gap. The results clearly represent that pure CuO, CuO-1La, CuO-3La, CuO-5La, and CuO-7La samples have band gap energy 2.59, 2.47, 2.10, 2.15, and 2.32 eV, respectively. The band gap energy is in the range of the visible light to utilize the solar spectrum as and when required.

The band gap was estimated from Tau'c plot depicted in Figure 6B using Equation (3)⁵¹:

$$(\alpha h\nu)^2 = A(h\nu - E_g)^n, \quad (3)$$

whereas A is the constant, α is the absorption coefficient, and $h\nu$ represents the incident photon energy. n denotes the transition, that is, 1 for direct transitions and $\frac{1}{2}$ for indirect transitions.

3.5 | PL analysis

PL analysis was utilized to explore optical characteristics of the synthesized nanostructures and the behavior of the charge carriers in response to light irradiation. The synthesized nanostructures were excited by 340 nm wavelength and the PL graph of the nanostructure is given in Figure 7. The graph shows that the intensity peaks and hence recombination rate are highest for the pure and CuO-1La samples, whereas it is least for the CuO-3La sample. The sharp intensity peaks can attribute to the large recombination rate which may be due to excessive oxygen vacancies resulting in less photocatalytic activity.⁵² Further, the broadness of peaks towards higher wavelength and in the visible region may be attributed due to the crystal defects by incorporation of La ions into matrix compounds. The analysis describes that the sample CuO-3La is the optimal sample which can exhibit a high photocatalytic activity.

4 | PHOTOCATALYSIS EVALUATION

CuO nanostructures represent the wide band gap and utilize UV light for photocatalysis with other practical implications. This study focuses on the incorporation of

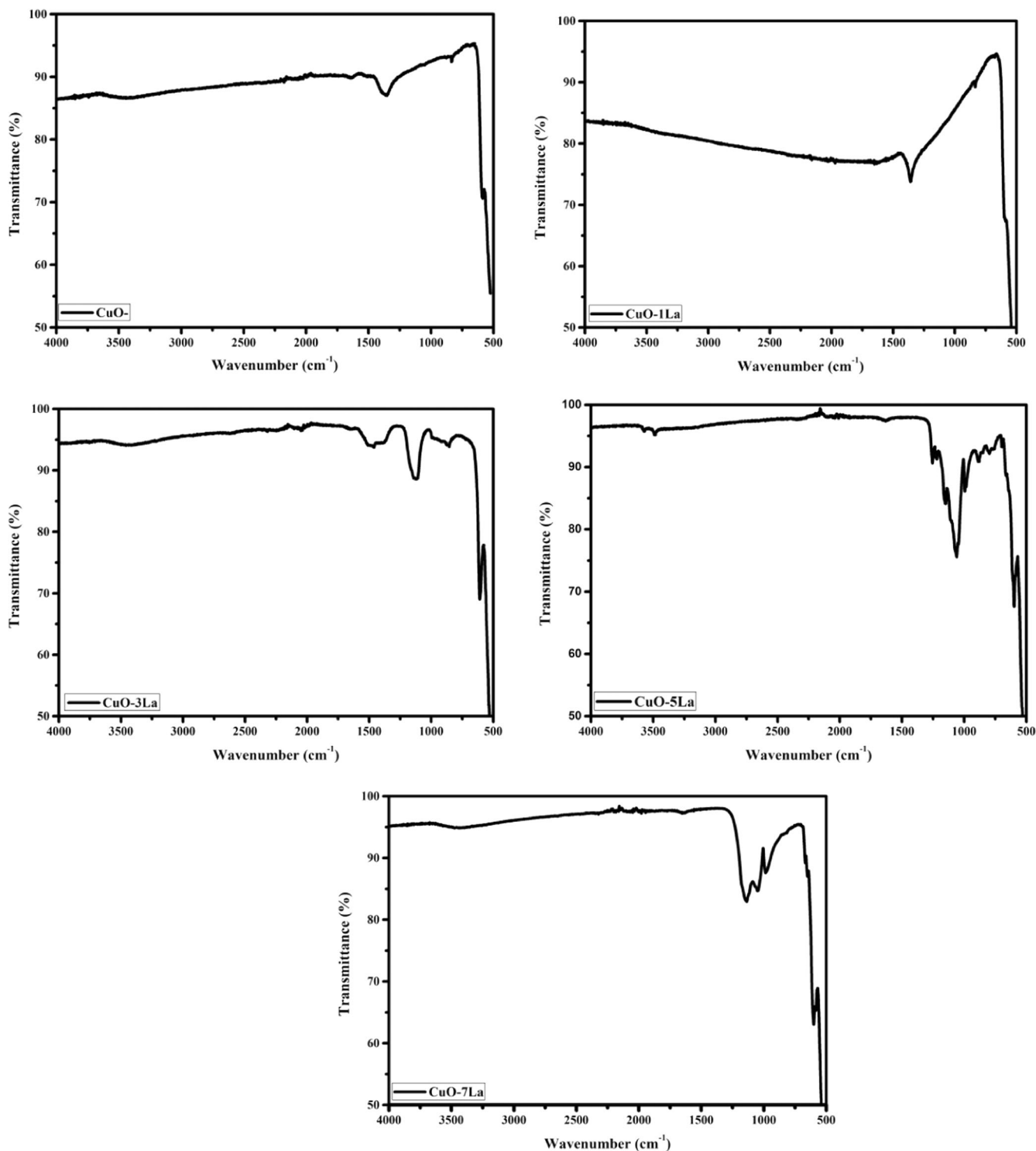


FIGURE 5 FTIR spectra of fabricated La-doped CuO nanostructures. FTIR, Fourier transform infrared.

La into CuO nanostructures to modify the morphology and optical characteristics to cater the visible light as well as the visible solar spectrum. The visible-light-driven photocatalyst could be a cost-effective and sustainable photocatalyst for water purifications, water splitting, and hydrogen energy production. In this study, synthesized pure CuO- and La-doped CuO nanophotocatalysts

exhibited visible-light-driven band gap and were utilized for MB dye removal under visible light exposure. The process of photocatalytic pollutant degradation is explained in Equations (4)–(10).⁴⁸ The effect of varying catalyst concentration, time of light irradiation, and pH was also examined to optimize the parameters. The process is described in the following sections:

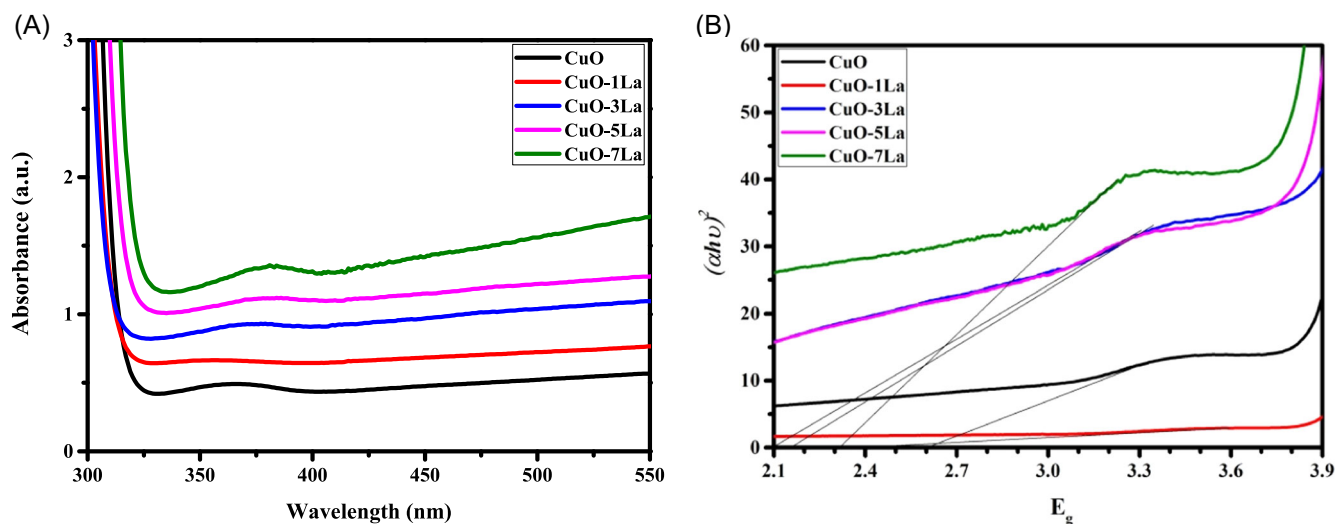


FIGURE 6 (A) Ultraviolet-visible absorption spectra of La-doped CuO nanostructures and (B) band gap spectra of La-doped CuO nanostructures.

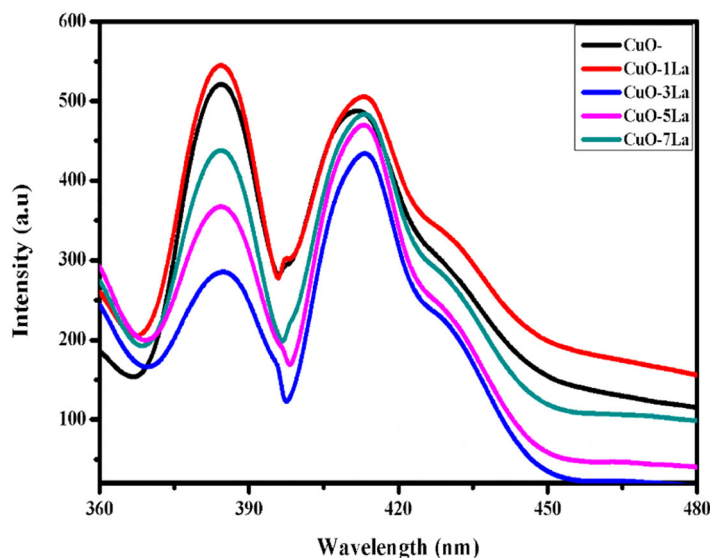
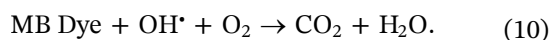
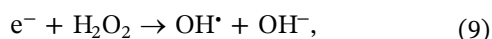
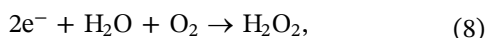
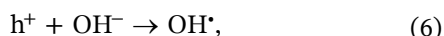
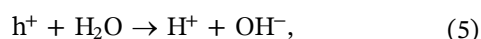
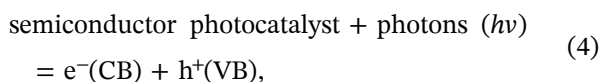


FIGURE 7 Photoluminescence spectra of La-doped CuO samples.



4.1 | Influence of light irradiation time

Photocatalytic performance of CuO- and La-doped CuO for removal of MB dye under the illumination of the visible light is depicted in Figure 8. The test dye samples have 6 ppm concentration and were treated with pure CuO- and La-doped CuO photocatalysts and samples were irradiated for 90 min. It may be perceived from the graph that the CuO-3La sample displayed the superior photocatalytic performance against MB dye with maximum efficiency greater than 97%. The degradation of MB dye with La-doped samples is found to be higher in comparison with the pure CuO, that is, may be due to higher surface/volume ratio. Further, the incorporation of La in pure CuO also produces crystal defects which

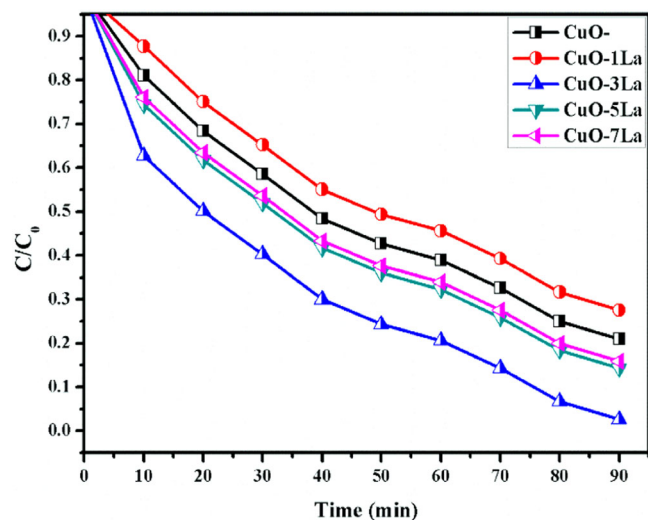


FIGURE 8 Influence of irradiation of light time on photocatalytic reduction of methylene blue dye.

generate shallow states, and with the light irradiation photogenerated electrons reside in these states for a longer period to accentuate the photocatalytic activity of catalysts materials.

4.2 | pH effect

Influence of pH on the photocatalytic elimination of MB dye is illustrated in Figure 9 which depicts that maximum degradation is achieved at pH=7. The maximum degradation at 7 pH was greater than 77% for sample CuO-3La. It is evident that when the La concentration was further increased the value of photocatalytic degradation against MB dye was decreased. The proficient degradation obtained for the optimal dopant may attribute to different factors. First, La can generate the oxygen vacancies which can be effective for trapping the photogenerated electrons, however, further increase in the La concentration can generate excessive oxygen vacancies on the catalyst surface creating a hotspot for the recombination of photogenerated carriers.⁴⁹ Second, the electronegativity difference can cause the transfer of electrons from the valence band, which can increase the photocatalytic activity.⁵⁰ Third, lattice deformation performs a significant part in the photocatalytic performance. La can cause crystal defects in CuO structure, which averts the charge carriers recombination causing enhancement in the photocatalytic activity.²³ However, increasing the concentration of dopant from optimal levels does not allow the material to diffuse but to remain on the surface, which hinders the passage of light and results in decrease in photocatalytic reduction.⁵³

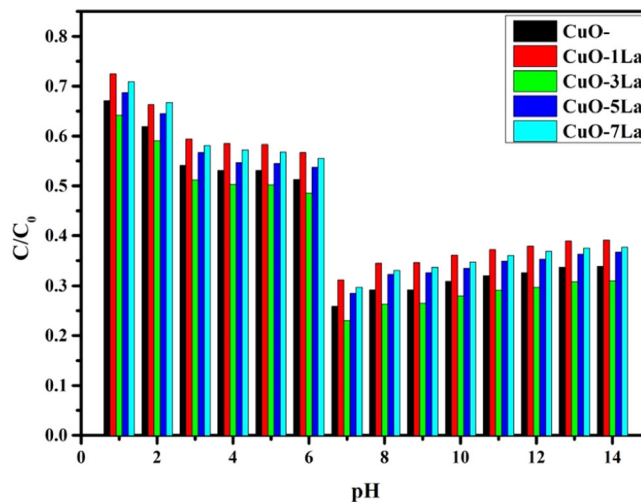


FIGURE 9 pH influence on photocatalytic removal of methylene blue dye.

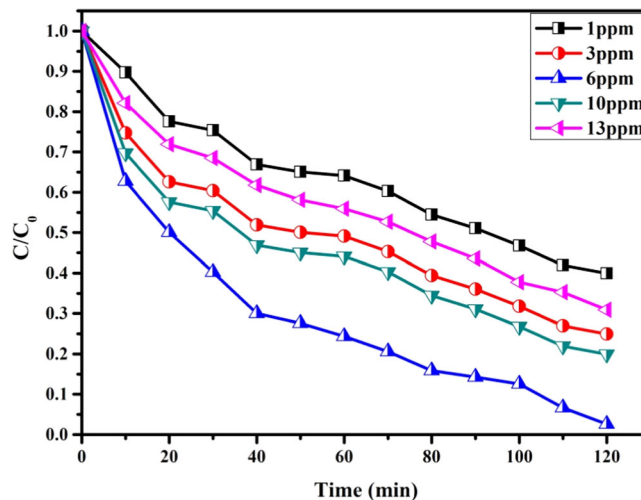


FIGURE 10 Catalyst loading influence on photocatalytic removal of methylene blue dye.

4.3 | Catalyst loading

Influence of catalyst loading on MB dye removal is depicted in Figure 10. Different concentrations of synthesized La-doped CuO nanophotocatalysts (i.e., 1, 3, 6, 10, and 13 ppm) were used to analyze the effect of nanophotocatalysts on photocatalytic reduction of MB dye. It can be observed that 6 ppm catalyst concentration exhibited proficient photocatalytic efficiency. All other catalyst concentrations also exhibited good photocatalytic results but increasing catalyst concentration causes a decrease in photocatalytic activity. This is because increasing catalyst concentration causes an increase in the recombination rate of electron-hole. This increase in

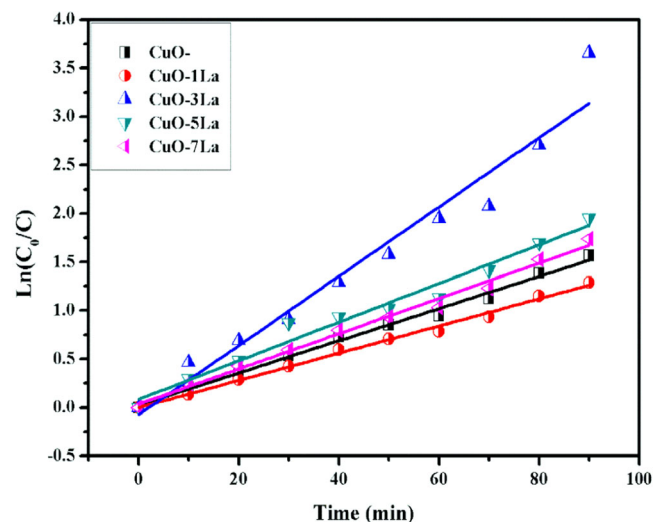


FIGURE 11 Kinetic study of as-synthesized samples against methylene blue dye.

the electron–hole recombination rate causes a decrease in photocatalytic activity. When the recombination rate increases the visible light does not degrade the MB dye, but at 6 ppm the recombination rate was much less that in turn increased the photocatalytic performance of La-doped CuO nanophotocatalysts.

4.4 | Kinetic study and cyclic stability

The photocatalytic degradation data were utilized to study the kinetics for dye reduction. Figure 11 shows the kinetics of manufactured pure CuO- and La-doped CuO photocatalysts against MB dye. The kinetics were calculated using the relation in Equation (11)⁴¹:

$$\ln\left(\frac{C_0}{C}\right) = kt. \quad (11)$$

Whereas C and C_0 are the dye concentrations and k denotes the reaction rate constant. The results represent the pseudo-first-order kinetics for the removal of the MB dye. The reaction rate for pure CuO and as-synthesized CuO-La photocatalysts is 0.0165, and 0.0143, 0.0359, 0.0199, and 0.0182 min^{-1} , correspondingly. It may clearly be observed that the reaction rate for CuO-3La is higher than all other photocatalysts.

The cyclic stability and reusability of photocatalysts are their ability to reuse it for multiple times in the degradation of a compound and dye. Figure 12 shows the cyclic stability of CuO-3La sample being the best sample among all synthesized samples. The photocatalyst is

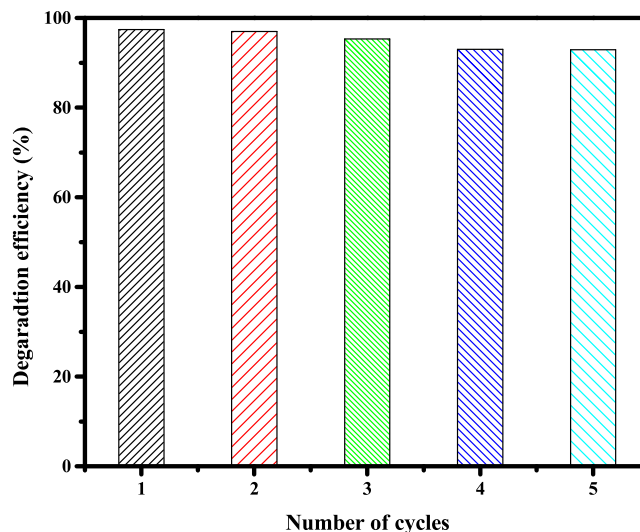


FIGURE 12 Cyclic stability of synthesized nanophotocatalysts for CuO-3La sample.

separated via centrifugation, then washed with deionized water and dried. The photocatalyst is applied to the dye solution again for the next cycle over the same time duration and other experimental conditions. The photocatalyst (CuO-3La) showed 92.88% stability for five cycles against MB dye which makes these photocatalysts very useful for commercial use and applications at large scale. Table 2 explains the comparison of previously reported La-doped CuO with the present research. It can be seen from Table 2 that photocatalyst prepared via the hydrothermal method exhibited higher photocatalytic efficiency than the reported literature. A small amount of photocatalyst effectively degraded the MB dye in a short period of time.

4.5 | Photocatalytic H₂ evolution

The photocatalytic evolution of the H₂ rate via H₂O splitting could be enhanced by the hybrid effect of CuO- and La-incorporated CuO nanomaterials. The bar graph plot of hydrogen production from water splitting for all constructed photocatalysts under solar irradiation is shown in Figure 13. The enhanced hydrogen production (98.5 $\mu\text{mol h}^{-1} \text{g}^{-1}$) was observed using 5% La/CuO nanomaterials and it was significantly higher than the former reports.⁵⁴ The outstanding performance for H₂ production via H₂O splitting causes the strong absorption of sunlight because of the minimum band gap which enables to form the electron–hole pair and their transport on the catalysts surface. The adsorbed H₂O on the surface split into H₂ and O₂.

TABLE 2 Comparison of La-doped CuO photocatalyst.

Photocatalyst	Synthesis method	Dye	Catalyst and dye concentration	Maximum degradation efficiency/rate constant	Reference
La-doped CuO	Solution combustion	MB dye	50 mg catalyst in 50 mL of 10 mg L ⁻¹ dye	~98% after in 90 min	37
La-doped CuO	Electrodeposition method	MB dye	1 cm × 1 cm catalyst in 12 mg L ⁻¹ dye	90.9%	36
La-doped ZnO	Electrospinning calcination	Rh B	1.5%	94.31% after 510 min	32
La-doped CuO	Hydrothermal method	MB dye	6 mg catalyst in 2.5 mg dye in 250 mL	Greater than 97% within 90 min with rate constant 0.0359 min ⁻¹	Present work

Abbreviations: MB, methylene blue; Rh, rhodamine.

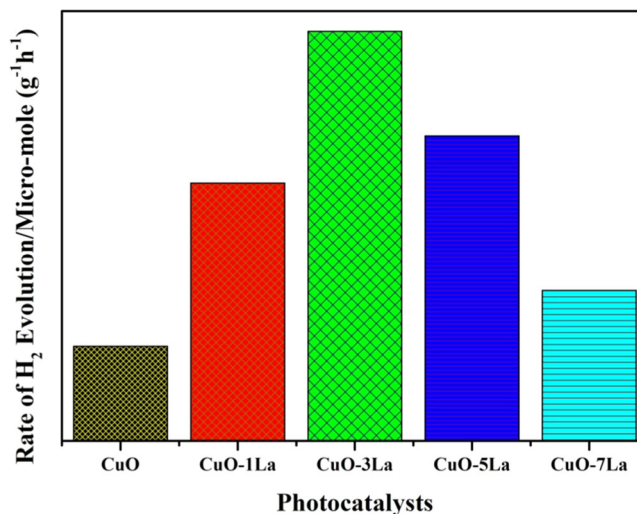


FIGURE 13 Hydrogen production from water splitting for all fabricated photocatalysts.

5 | CONCLUSION

Pure CuO- and La-doped CuO nanostructures were prepared effectively via a facile, cost-efficient hydrothermal approach for photocatalytic applications. The pure CuO nanostructures were modified by the doping of La to govern the morphology and other properties. The fabricated nanostructures showed a 2.10–2.59 eV band gap which is capable to cater the visible light and the visible solar spectrum. The pure and doped CuO nanostructures were crystalline in nature and showed 15–25 nm crystallite size which was further decreased by increasing the doping of the La. The needle-like morphology was obtained with optimal doping to exhibit the highest surface area for higher photocatalytic characteristics. Further, the photocatalytic properties of the pure and La-doped CuO nanostructures were optimized for MB dye with different experimental conditions. The synthesized CuO-3La photocatalyst exhibited excellent photocatalytic performance of dye degradation and hydrogen production 95.3 μmol h⁻¹ g⁻¹ with more than 97% excellent cyclic stability. Therefore, it can be summarized that the synthesized nanophotocatalysts could be utilized for water purification, water splitting, and hydrogen generation at large and commercial scales.

ACKNOWLEDGMENTS

The authors extend their appreciation to the Researchers Supporting Project number (RSPD2023R698), King Saud University, Riyadh, Saudi Arabia for funding this research work.

CONFLICT OF INTEREST STATEMENT

The authors declare no conflict of interest.

ORCID

Muhammad Rafique  <http://orcid.org/0000-0002-2538-2768>

Waqar Muhammad Ashraf  <http://orcid.org/0000-0003-1841-7659>

REFERENCES

- Kyzas GZ, Mitropoulos AC. Nanomaterials and nanotechnology in wastewater treatment. *Nanomaterials*. 2021;11(6):1539.
- Ma X, Zhao S, Tian Z, et al. MOFs meet wood: reusable magnetic hydrophilic composites toward efficient water treatment with super-high dye adsorption capacity at high dye concentration. *Chem Eng J*. 2022;446:136851.
- Yang W, Wang Y, Wang Q, et al. Magnetically separable and recyclable Fe₃O₄@PDA covalent grafted by L-cysteine core-shell nanoparticles toward efficient removal of Pb₂₊. *Vacuum*. 2021;189:110229.
- Jian S, Shi F, Hu R, et al. Electrospun magnetic La₂O₃-CeO₂-Fe₃O₄ composite nanofibers for removal of fluoride from aqueous solution. *Compos Commun*. 2022;33:101194.
- Obey G, Adelaide M, Ramaraj R. Biochar derived from non-customized matamba fruit shell as an adsorbent for wastewater treatment. *J Bioresour Bioprod*. 2022;7(2):109-115.
- Sibhatu AK, Weldegebriale GK, Sagadevan S, Tran NN, Hessel V. Photocatalytic activity of CuO nanoparticles for organic and inorganic pollutants removal in wastewater remediation. *Chemosphere*. 2022;300:134623.
- Jjagwe J, Olupot PW, Menya E, Kalibbala HM. Synthesis and application of granular activated carbon from biomass waste materials for water treatment: a review. *J Bioresour Bioprod*. 2021;6(4):292-322.
- Bilińska L, Gmurek M, Ledakowicz S. Textile wastewater treatment by AOPs for brine reuse. *Process Saf Environ Prot*. 2017;109:420-428.
- Meek ME. AOPs in hazard characterization for human health. *Curr Opin Toxicol*. 2017;3:80-86.
- Nadeem K, Guyer GT, Dizge N. Polishing of biologically treated textile wastewater through AOPs and recycling for wet processing. *J Water Process Eng*. 2017;20:29-39.
- Ganguly P, Harb M, Cao Z, et al. 2D nanomaterials for photocatalytic hydrogen production. *ACS Energy Lett*. 2019;4(7):1687-1709. doi:10.1021/acsenergylett.9b00940
- Zeid EFA, Ibrahim IA, Mohamed WAA, Ali AM. Study the influence of silver and cobalt on the photocatalytic activity of copper oxide nanoparticles for the degradation of methyl orange and real wastewater dyes. *Mater Res Express*. 2020;7(2):026201.
- Rostami A, Atashkar B, Gholami H. Novel magnetic nanoparticles Fe₃O₄-immobilized domino Knoevenagel condensation, Michael addition, and cyclization catalyst. *Catal Commun*. 2013;37:69-74.
- Rafique M, Shafiq F, Ali Gillani SS, Shakil M, Tahir MB, Sadaf I. Eco-friendly green and biosynthesis of copper oxide nanoparticles using *Citrofortunella microcarpa* leaves extract for efficient photocatalytic degradation of Rhodamin B dye form textile wastewater. *Optik*. 2020;208:164053.
- Zaman S, Zainelabdin A, Amin G, Nur O, Willander M. Efficient catalytic effect of CuO nanostructures on the degradation of organic dyes. *J Phys Chem Solids*. 2012;73(11):1320-1325. doi:10.1016/j.jpcs.2012.07.005
- Feng Y, Zheng X. Plasma-enhanced catalytic CuO nanowires for CO oxidation. *Nano Lett*. 2010;10(11):4762-4766.
- Dhilip Kumar R, Sreevani K, Radhika G, et al. One-pot synthesis of CuO-Cu₂O nanoscrubbers for high-performance pseudo-supercapacitors applications. *Mater Sci Eng B*. 2022;281:115755.
- Nagarani S, Sasikala G, Yuvaraj M, Kumar RD, Balachandran S, Kumar M. ZnO-CuO nanoparticles enameled on reduced graphene nanosheets as electrode materials for supercapacitors applications. *J Energy Storage*. 2022;52:104969.
- Cuong HN, Pansambal S, Ghotekar S, et al. New frontiers in the plant extract mediated biosynthesis of copper oxide (CuO) nanoparticles and their potential applications: a review. *Environ Res*. 2022;203:111858.
- Kidowaki H, Oku T, Akiyama T. Fabrication and characterization of CuO/ZnO solar cells. *J Phys: Conf Ser*. 2012;1:012022.
- Wang L, Zhang K, Hu Z, Duan W, Cheng F, Chen J. Porous CuO nanowires as the anode of rechargeable Na-ion batteries. *Nano Res*. 2014;7(2):199-208.
- Govenius J, Lake RE, Tan KY, Möttönen M. Detection of zeptojoule microwave pulses using electrothermal feedback in proximity-induced Josephson junctions. *Phys Rev Lett*. 2016;117(3):030802.
- Iqbal T, Masood A, Khalid NR, Tahir MB, Asiri AM, Alrobei H. Green synthesis of novel lanthanum doped copper oxide nanoparticles for photocatalytic application: correlation between experiment and COMSOL simulation. *Ceram Int*. 2022;48(10):13420-13430. doi:10.1016/j.ceramint.2022.01.160
- Xu L, Zheng G, Pei S, Wang J. Investigation of optical bandgap variation and photoluminescence behavior in nanocrystalline CuO thin films. *Optik*. 2018;158:382-390.
- Chandrasekar M, Subash M, Logambal S, et al. Synthesis and characterization studies of pure and Ni doped CuO nanoparticles by hydrothermal method. *J King Saud Univ—Sci*. 2022;34(3):101831.
- McFarland EW, Metiu H. Catalysis by doped oxides. *Chem Rev*. 2013;113(6):4391-4427.
- Youcef R, Benhadji A, Zerrouki D, Fakhakh N, Djelal H, Taleb Ahmed M. Electrochemical synthesis of CuO-ZnO for enhanced the degradation of brilliant blue (FCF) by sono-photocatalysis and sonocatalysis: kinetic and optimization study. *React Kinet Mech Catal*. 2021;133:541-561.
- Liu Q, Deng W, Wang Q, et al. An efficient chemical precipitation route to fabricate 3D flower-like CuO and 2D leaf-like CuO for degradation of methylene blue. *Adv Powder Technol*. 2020;31(4):1391-1401.
- Anu Prathap MU, Kaur B, Srivastava R. Hydrothermal synthesis of CuO micro-/nanostructures and their applications in the oxidative degradation of methylene blue and non-enzymatic sensing of glucose/H₂O₂. *J Colloid Interface Sci*. 2012;370(1):144-154.

30. Liqiang J, Xiaojun S, Baifu X, Baiqi W, Weimin C, Honggang F. The preparation and characterization of La doped TiO₂ nanoparticles and their photocatalytic activity. *J Solid State Chem.* 2004;177(10):3375-3382.
31. Yang W, Shi F, Jiang W, et al. Outstanding fluoride removal from aqueous solution by a La-based adsorbent. *RSC Adv.* 2022;12(47):30522-30528.
32. Jian S, Tian Z, Hu J, et al. Enhanced visible light photocatalytic efficiency of La-doped ZnO nanofibers via electrospinning-calcination technology. *Adv Powder Mater.* 2022;1(2):100004.
33. Varughese G, Rini V, Suraj SP, Usha KT. Characterisation and optical studies of copper oxide nanostructures doped with lanthanum ions. *Adv Mater Sci.* 2014;14(4):49-60.
34. Devi LV, Selvalakshmi T, Sellaiyan S, Uedono A, Sivaji K, Sankar S. Effect of La doping on the lattice defects and photoluminescence properties of CuO. *J Alloys Compd.* 2017;709:496-504.
35. Devi LV, Sellaiyan S, Sankar S, Sivaji K. Structural and optical investigation of combustion derived La doped copper oxide nanocrystallites. *Mater Res Express.* 2018;5(2):024002.
36. Yan B, Wang Y, Jiang T, Wu X. Synthesis and enhanced photocatalytic property of La-doped CuO nanostructures by electrodeposition method. *J Mater Sci: Mater Electron.* 2016;27(5):5389-5394.
37. Rodney JD, Deepapriya S, Annie Vinosha P, et al. Photofenton degradation of nano-structured La doped CuO nanoparticles synthesized by combustion technique. *Optik.* 2018;161:204-216.
38. Jian S, Cheng Y, Ma X, et al. Excellent fluoride removal performance by electrospun La-Mn bimetal oxide nanofibers. *New J Chem.* 2022;46(2):490-497.
39. Jian S, Chen Y, Shi F, et al. Template-free synthesis of magnetic La-Mn-Fe tri-metal oxide nanofibers for efficient fluoride remediation: kinetics, isotherms, thermodynamics and reusability. *Polymers.* 2022;14(24):5417.
40. Singh V, Bansal P. Fabrication and characterization of needle shaped CuO nanoparticles and their application as photocatalyst for degradation of organic pollutants. *Mater Lett.* 2020;261:126929.
41. Chauhan M, Kaur N, Bansal P, Kumar R, Srinivasan S, Chaudhary GR. Proficient photocatalytic and sonocatalytic degradation of organic pollutants using CuO nanoparticles. *J Nanomater.* 2020;2020:1-15.
42. Karthikeyan N, Narayanan V, Stephen A. Synthesis and characterization of coupled ZnO/Ag/CuO nanomaterials for photocatalytic degradation of organic dye under UV irradiation. *Int J Inn Res Sci Eng.* 2014;2:74-79.
43. Mehr ES, Sorbiun M, Ramazani A, Fardood ST. Plant-mediated synthesis of zinc oxide and copper oxide nanoparticles by using ferulago angulata (schlecht) boiss extract and comparison of their photocatalytic degradation of Rhodamine B (RhB) under visible light irradiation. *J Mater Sci: Mater Electron.* 2018;29(2):1333-1340.
44. Wang Y, Jiang T, Meng D, Wang D, Yu M. Synthesis and enhanced photocatalytic property of feather-like Cd-doped CuO nanostructures by hydrothermal method. *Appl Surf Sci.* 2015;355:191-196.
45. Sonia S, Jose Annsi I, Suresh Kumar P, Mangalaraj D, Viswanathan C, Ponpandian N. Hydrothermal synthesis of novel Zn doped CuO nanoflowers as an efficient photodegradation material for textile dyes. *Mater Lett.* 2015;144:127-130.
46. Sunitha M, Karthik AD, Geetha K. Eco synthesis, spectral and antimicrobial studies of copper oxide (CuO) nanoparticles. *Mater Today: Proc.* 2020;29:1229-1234.
47. Ca NX, Van HT, Do PV, et al. Influence of precursor ratio and dopant concentration on the structure and optical properties of Cu-doped ZnCdSe-alloyed quantum dots. *RSC Adv.* 2020;10(43):25618-25628.
48. Viswanathan B. Photocatalytic degradation of dyes: an overview. *Curr Catal.* 2018;7(2):99-121.
49. Xin B, Wang P, Ding D, Liu J, Ren Z, Fu H. Effect of surface species on Cu-TiO₂ photocatalytic activity. *Appl Surf Sci.* 2008;254(9):2569-2574.
50. Li Y, Peng S, Jiang F, Lu G, Li S. Effect of doping TiO₂ with alkaline-earth metal ions on its photocatalytic activity. *J Serb Chem Soc.* 2007;72(4):393-402.
51. Rafique M, Rafique MS, Butt SH, et al. Dependence of the structural optical and thermo-physical properties of gold nano-particles synthesized by laser ablation method on the nature of laser. *Optik.* 2017;134:140-148.
52. Khalid NR, Hammad A, Tahir MB, et al. Enhanced photocatalytic activity of Al and Fe co-doped ZnO nanorods for methylene blue degradation. *Ceram Int.* 2019;45(17):21430-21435.
53. Riaz N, Kait CF, Man Z, Dutta BK, Ramli RM, Khan MS. Visible light photodegradation of azo dye by Cu/TiO₂. In: Ismail L, Azizli KA, Murugesan T, Ganguly S, Uemura Y, eds. *Advanced Materials Research.* Trans Tech Publ; 2014: 151-159.
54. Rodney JD, Deepapriya S, Cyril Robinson M, et al. Lanthanum doped copper oxide nanoparticles enabled proficient bifunctional electrocatalyst for overall water splitting. *Int J Hydrogen Energy.* 2020;45(46):24684-24696. doi:10.1016/j.ijhydene.2020.06.240

How to cite this article: Rafique M, Khalid NR, Irshad M, et al. Visible light-active pure and lanthanum-doped copper oxide nanostructures for photocatalytic degradation of methylene blue dye and hydrogen production. *Energy Sci Eng.* 2023;1-13. doi:10.1002/ese3.1476